

AL-TR-90-018

AD:

2



AD-A225 504

DTIC FILE COPY

Final Report
for the period
February 1987 to
February 1990

Investigations of Hypervalent Compounds as High-Energy Materials

DTIC
ELECTE
AUG 22 1990
S D
cc

June 1990

Chemical Physics Institute
University of Oregon
Eugene OR 97403

F04611-87-K-0021

Approved for Public Release

Distribution is unlimited. The AL Technical Services Office has reviewed this report, and it is releasable to the National Technical Information Service, where it will be available to the general public, including foreign nationals.

Prepared for the: **Aeronautics Laboratory (AFSC)**
Air Force Space Technology Center
Space Systems Division
Air Force Systems Command
Edwards AFB CA 93523-5000

90 08 21 062

TABLE OF CONTENTS

Introduction	1
Scientific Background.....	4
HNO ⁻	4
NH ₄ ⁻	4
SiH ₅ ⁻	5
CH ₅ ⁻	5
Equipment Design.....	6
Fast Coaxial Ion Beam.....	6
Slow Coaxial Molecular Ion Beam.....	10
Source Development.....	10
Branscomb-type Source	10
Bowen-type Source.....	10
Corona-Excited Supersonic Expansion	14
Results	14
Molecules	14
HNO ⁻	14
NH ₄ ⁻	17
CH ₅ ⁻	17
SiH ₅ ⁻	23
Other Technical Advances	23
Photodissociation.....	23
Photodetachment.....	23
Experimental Techniques.....	23
Conclusions	25
Publications.....	26
References	27

LIST OF FIGURES

Figure 1a.	Typical reaction path showing a single energetic maximum at the transition state.....	2
Figure 1b.	Reaction path with a local minimum near the energy maximum.....	2
Figure 2a.	Two reaction surfaces.....	3
Figure 2b.	Interacting potential surfaces intersecting as in 2a	3
Figure 3.	Fast ion beam system	7
Figure 4.	The interaction region.....	9
Figure 5.	Coaxial interaction region of the slow molecular ion beam.....	11
Figure 6.	Branscomb-type ion source	12
Figure 7.	Operation of the skimmer in a high-pressure nozzle source.....	13
Figure 8.	Energy levels of HNO^- (left) and HNO (right).....	15
Figure 9.	Transitions observed in the spectrum of HNO^-	16
Figure 10.	Linewidths observed as a function of quantum level.....	20
Figure 11.	Permissible HNO^- geometries	21
Figure 12.	Mass spectrum showing the NH_4^- anion (mass 18) prepared in a nozzle expansion of H_2 and ammonia	22
Figure 13.	Ions found on axis in skimmed plasma beam	24

LIST OF TABLES

Table I.	Effective rotational constants for the ν_1 band of HNO^-	18
Table II.	Matrix elements of the A reduced effective rotational and spin-rotation Hamiltonian.....	19

Introduction

Interest in hypervalent ions stems from the need to understand how to lock energy into molecules in amounts greater than heretofore attainable.

The basic idea generalizes the concept of "Lake Eyring," a metastable depression near the crest of a reaction pathway.

In a reaction, for example, an SN2 substitution, there is generally an energy barrier over which the reaction must proceed (Figure 1a). There is no reason that only one barrier should occur, and double barriers could lead to the existence of a metastable reaction intermediate (Fig. 1b). Since this depression would be at the top of a reaction path, it could conceivably contain a very energetic metastable species.

Recent theoretical work points to one mechanism for generating such a situation. Suppose that, in addition to the ground state potential surface reaching a maximum at its transition state, as represented by Figure 1a, there is an additional excited state surface that reaches its minimum in the same vicinity along the reaction coordinate. For example, this excited state may represent a different electronic configuration. This situation is depicted in Figure 2a. If the excited surface intersects the ground electronic surface, and if electronic mixing of the excited state with the ground state occurs, this situation will lead to the separation of the two adiabatic surfaces as shown in Figure 2b. In a natural way, this constructs a dimple in the ground state reaction curve near the reaction maximum.

This method of forming a metastable minimum allows some control over the shape of this depression. The critical parameters controlling the formation of this depression are those of the height of the maximum energy along the ground state reaction path, and the height of the minimum energy along the excited state surface. Presumably, these parameters might be "tuned" chemically by the choice of the reacting atoms out of a series of similar reactants.

Recent theoretical results [1-4], and some experimental hints [5,6], suggest that such species actually do exist. For example, in the SN2 reaction of hydride, H^- , with ammonia, NH_3 , a four-hydrogen intermediate may form in which all hydrogens are symmetrically bound about a tetrahedral nitrogen center. The approach of the hydride on the lower reaction surface involves ten electrons,--two too many for the four bonding orbitals available from the nitrogen valence shell 2s and 2p orbitals and the four 1s hydrogen orbitals. As the hydride approaches the nitrogen, one pair of the electrons is in a valence orbital that becomes anti-bonding. Thus, the ground state reaction surface involving only these valence configurations is repulsive, except for a weak, long-range ion-dipole interaction [7-9]. If this were all there were to the situation, a "normal" reaction surface would obtain, as in Figure 1a. But this is not the whole situation. Calculations [1-4] indicate that at the tetrahedral geometry, because of the high stability of the NH_4^+ ammonium ion, a lower energy configuration occurs, described as an ammonium core with two electrons in an outer 3s orbital--a "double-Rydberg" configuration. At large reactant separation, the surface for this configuration corresponds to that of H^- approaching NH_3^{**} , the latter with two non-bonding nitrogen electrons promoted into an outer 3s Rydberg orbital--quite high energy for the separated reactants. The vacancy on the nitrogen may form a bonding combination with the occupied H^- orbital. This gives an attractive excited state surface. Thus, the curves shown in Figure 2 seem to apply, and it may be expected that a metastable depression forms near the reaction maximum. Indeed, calculations predict that this high energy, double-Rydberg form of NH_4^- is metastable with respect to nuclear distortions.

Our endeavor has been the study of a series of chemically similar species which are relevant to understanding the formation of such metastable molecules. We are interested in determining the conditions for forming the minimum on the reaction surface. All of the species of interest are those which may be thought of as occurring in SN2 reactions of hydride H^- with a neutral reaction center. These interesting species are intermediates in reactions such as

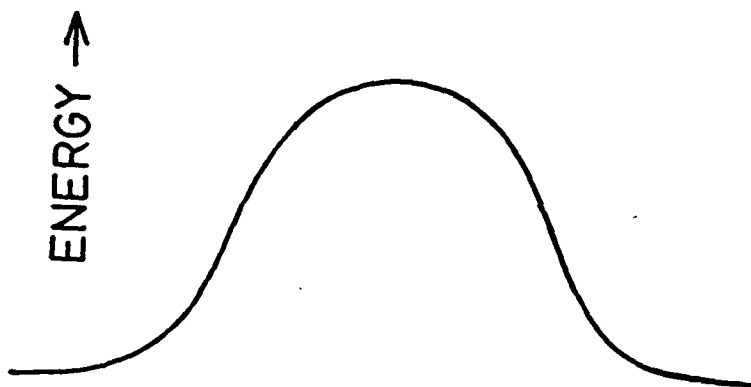


Figure 1a. Typical reaction path showing a single energetic maximum at the transition state. Only reactants on the left and products on the right are stable.

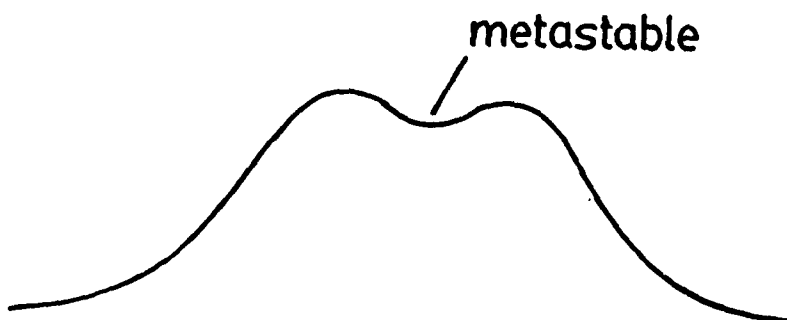


Figure 1b. Reaction path with a local minimum near the energy maximum. If the local minimum is deep enough, it may be possible to trap a metastable species for long periods of time in this "Lake Eyring."

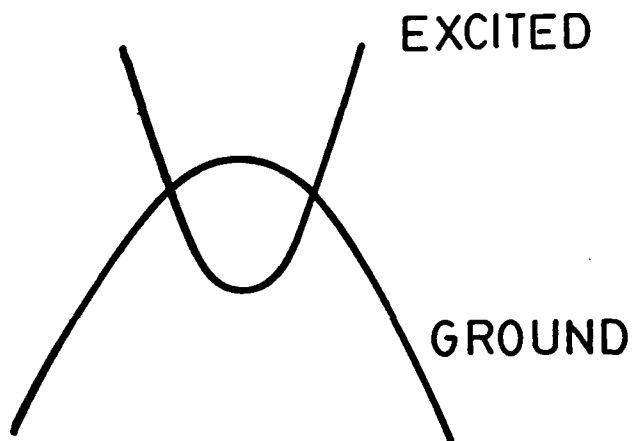


Figure 2a. Two reaction surfaces, one from the ground electronic configuration, and one from an excited electronic configuration, showing how crossing may be possible near the energetic transition state. If interaction between the surfaces is not allowed, such as if they represent different electronic symmetries, the ground state still has a single energy maximum.

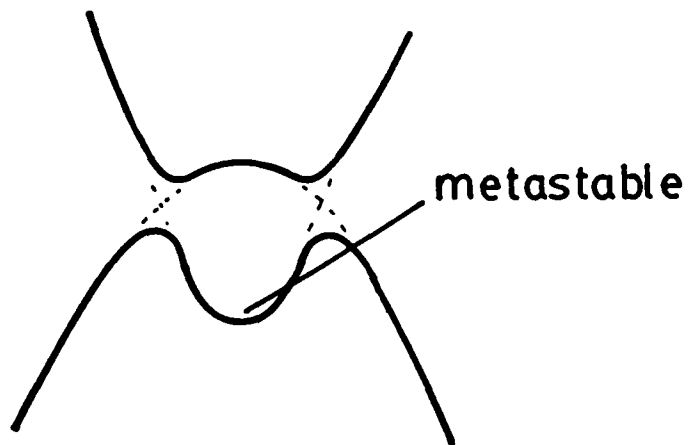


Figure 2b. Interacting potential surfaces intersecting as in 2a, now showing the formation of an energetic local minimum on the ground state adiabatic surface in the vicinity of the transition state.



Our focus is on the reaction intermediates, and the exciting prospect of isolating these as energetic, metastable species. Intentionally, a range of central atoms and types of coordination geometries have been chosen to discern the chemical requirements for the formation of energetic metastable intermediates.

The storage of energy in high valence states is well known--for example, the perchlorate ion ClO_4^- is a standard oxidizer component of propellants, in which the energy content of ammonium perchlorate salt is about 20 kJ/mole greater than that of ammonium chloride and gaseous oxygen [10]. There the chlorine is in a high valence state of 7. It may be possible to form energetic states, as outlined above, in which the central atom is an even more energetic, hypervalent species, normally only associated with a reaction transition state. It is such hypervalent configurations, and the conditions under which these may be stabilized, which form the basis of the study performed here.

Scientific Background

HNO^-

The only prior study of HNO^- was that of Ellis and Ellison [11] who resolved the energy of the photoelectrons detached by 488 nm light from an argon ion laser. These authors measured the electron affinities of HNO and DNO as 0.338(15) and 0.330(15) eV, respectively, or slightly greater than 2700 cm^{-1} . The molecule will therefore autodetach from a single vibration in the $v_1 = 1$ state. From a hot band of the ion, they also determined a wavenumber of 1153 (170) cm^{-1} for the v_2 bending vibration of HNO^- . This is significantly less than the value of 1550 cm^{-1} for the neutral HNO , and suggests significant weakening of NO bond in the anion.

The HNO^- ion is expected to be sharply bent in its ground electronic state. The low mass of the hydrogen atom, however, causes the rotational Hamiltonian to differ only slightly from that of a prolate symmetric rotor. The ground state is expected to be X^2A'' , with single HN and NO bonds; from an analysis based upon the Franck-Condon progression of shifted harmonic oscillators, Ellis and Ellison estimate the N-O bond length has increased to 1.33 Angstroms in the ion, compared to 1.242 Angstroms in the neutral.

There is little theoretical guidance in the open literature on this species.

NH_4^-

Information on the reactivity and energetics of NH_4^- has been obtained through ICR [6,13], and photodetachment experiments [5]. The small hydride affinity of ammonia (-25 kJ/mol) [14] and the electron affinity, differing little from that of H^- , suggest that the structure of observed NH_4^- is that of weakly bound H^- and NH_3 units. There is now some weak evidence, based upon photoelectron spectrometry, for the existence of a higher-energy metastable state [5,2].

Calculations are more optimistic about the existence of a high energy form of NH_4^- , stabilized exactly through the mechanism we have outlined. The low energy form is found [7-9], but a number of workers report the formation of a metastable, higher energy form [1-

4]. In this structure, a pair of electrons are located in a predominantly 3s orbital surrounding a stable NH_2^+ ammonium ion core. For small distortions this core is stable, but with large displacements of one of the hydrogens, the lower energy state corresponds to a valence NH_2H^- configuration.

Identification of the high energy metastable form, in the presence of the lower energy form, would have to take advantage of the spectral differences resulting from the differing geometries, since both ions would have the same mass. The low energy form could be expected to have a photodetachment threshold nearly that of hydride itself, and this is seen in the PES of negative ion beams of these ions [5]. Because of electronic reorganization, especially the promotion of the orbital containing the extra electron to 3s, one may expect the electron affinity of this ion to be less than that of the hydride. This agrees with what is found for the EA trend in calculations.

In addition to phototreshold differences, the overall structure found in the electronic spectra of the low energy and high energy forms should differ. The high-energy metastable form should have its photodetachment/photodissociation spectrum structured by broad $3s \rightarrow np$ Rydberg-like electronic promotions and sharp, double-Rydberg promotions [4], while the H^-NH_2 species should evidence almost an ordinary H^- photodetachment, slowly rising from zero at threshold according to a nearly Wigner $E^{(s/2)}$ power law (vide infra), with possibly structure added by an "atom-ligand" transfer band at the energy of the promotion of the H^- electron to the lowest unoccupied ammonia orbital. This charge transfer band probably would be located in the 1.5-2.7 eV region. Further identification of the ion would come from the vibrational and rotational fine-structure of the predissociation bands.

In both the visible and IR region of the spectrum, the NH_2H^- ion could be identified by its destruction into H^- and NH_2 , due to the low energy of the bonding. The high energy form should have available the additional pathway of $\text{NH}_2^- + \text{H}_2$ dissociation, which could be used to identify this ion's presence.

SiH_5^-

D.J. Hadjdasz and R.R. Squires [15] have demonstrated the existence of SiH_5^- in a flowing afterglow, prepared by hydride transfer from alkylsilyl hydride anions. This species is quite interesting with respect to the question of stability of hypervalent species because it is kinetically stable, but thermodynamically unstable, to the reaction



This has been demonstrated by catalytic decomposition in the flow tube. The calculated exothermicity is about 25 kJ/mol [16-21]. The geometry of the intermediate formed by hydride attack on silane involves equivalence of the approaching hydride with one or more of the SiH_4 hydrogens, since isotopic exchange occurs. All of the hydrogens appear to be involved, suggesting a low barrier for pseudorotation in agreement with calculations.

Two types of experiments could provide further information on this species. One type of experiment involves the IR excitation of an internal hydrogen motion, with the resulting absorption followed by loss of SiH_4^- through H_2 elimination. The second would involve visible/UV excitation. The SiH_5^- D_{3h} structure is expected to have a $(1a_1')^2(1a_2'')^2(1e')^4(2a_1')^2$ configuration, with empty $3a_1'$, $2e'$ and $2a_2''$ valence orbitals available for excitation. Thus, one or more visible or near UV transitions are expected for SiH_5^- , usable for providing information about this anion spectroscopically.

CH_5^-

The most difficult to produce and speculative of all of these species is expected to be the methane hydride anion. In terms of forming hypervalent excited states, this may be

the exception that proves the rule. There is no experimental evidence for its existence. The report of the analogous CBr_4^- was soon followed by an X-ray crystal structure showing the anion to be of the form $\text{CBr}_4 \cdot \text{Br}^-$ [22].

This CH_5^- anion is expected to be exactly opposite its silicon analogue in these respects: it is thermodynamically stable against H_2 elimination, but unstable to H^- elimination.

When we first began our work, we expected the geometry of this species to reflect the weakly bound $\text{H}^- \cdot \text{CH}_4$ [3,7,18,23-35]. Recently, calculations [4] have indicated that there is a metastable "double-Rydberg" state of CH_5^- about 0.3 eV below the neutral of the same geometry, and thus is stable to both autodetachment and metastable to hydride loss. There should be low lying metastable excitations (decaying by auger processes) at 1.8 and 3 eV above this.

Spectroscopically, the low energy form and the high energy form (if it exists) should be identifiable by the difference in their photodestruction spectra: the low energy "solvated" methane-hydride ion should have its detachment resembling that of H^- in both shape and intensity, while the high-energy "double-Rydberg" species should have its spectrum highly structured by metastable resonances [4], and with a much sharper threshold corresponding to detachment from a more diffuse 3s orbital.

Equipment Design

The major thrust behind the spectroscopic investigations of these ions was to attempt their investigation in the existing fast, coaxial ion beam, while leap-frogging technology to construction of a low energy energy coaxial molecular beam. The fast molecular ion beam has the advantages of being well understood technology, but is optimized for only CW lasers. The slow molecular beam, coupled with a pulsed time-of-flight mass spectrometer has the advantage of being usable with versatile pulsed lasers, but has the drawback of having not been constructed before.

The basic plan in both of these apparatuses is to obtain the wavelength dependent absorption spectrum by monitoring the disappearance of the ions in the beam when hit by a coaxial laser beam.

Fast Coaxial Ion Beam

A thorough description of the fast ion beam has been given by Harold Miller in the thesis prepared under this project [36]. A diagram is given in Figure 3.

The interaction region and laser system is pictured in Figure 4. The interaction region is contained in a large stainless steel chamber with copper and aluminum vacuum seals used exclusively. The pressure in this region is maintained at a few $\times 10^{-9}$ Torr by a 200 1/s ion pump making it unlikely that the negative ion beam will be significantly degraded by collisions with the background gas. The mean free path of a particle at this pressure is about a thousand miles.

A mass selected ion beam entering the interaction region passes through an einzel lens and vertical deflector, then is bent 90° in the horizontal plane by an electrostatic quadrupole ion beam bender. The geometry of the beam bender allows a laser beam to be merged coaxially with the ion beam as it turns the corner. The quadrupole, located about four feet from the ion source, rids the beam of any neutral particles created by collisions with background gas in the higher pressure extraction and Wien filter regions.

The beam bender pole pieces were made by quartering a 4.5 inch O.D., 5 inch long aluminum tube lengthwise. Each of the pole pieces were inverted lengthwise and placed so that their inner edges fell on a 3 inch diameter circle. The poles were then mounted on insulating sapphire balls and sandwiched between two parallel plates that hold the assembly together. Equal voltages are applied to diagonally opposed pole pieces. A voltage of

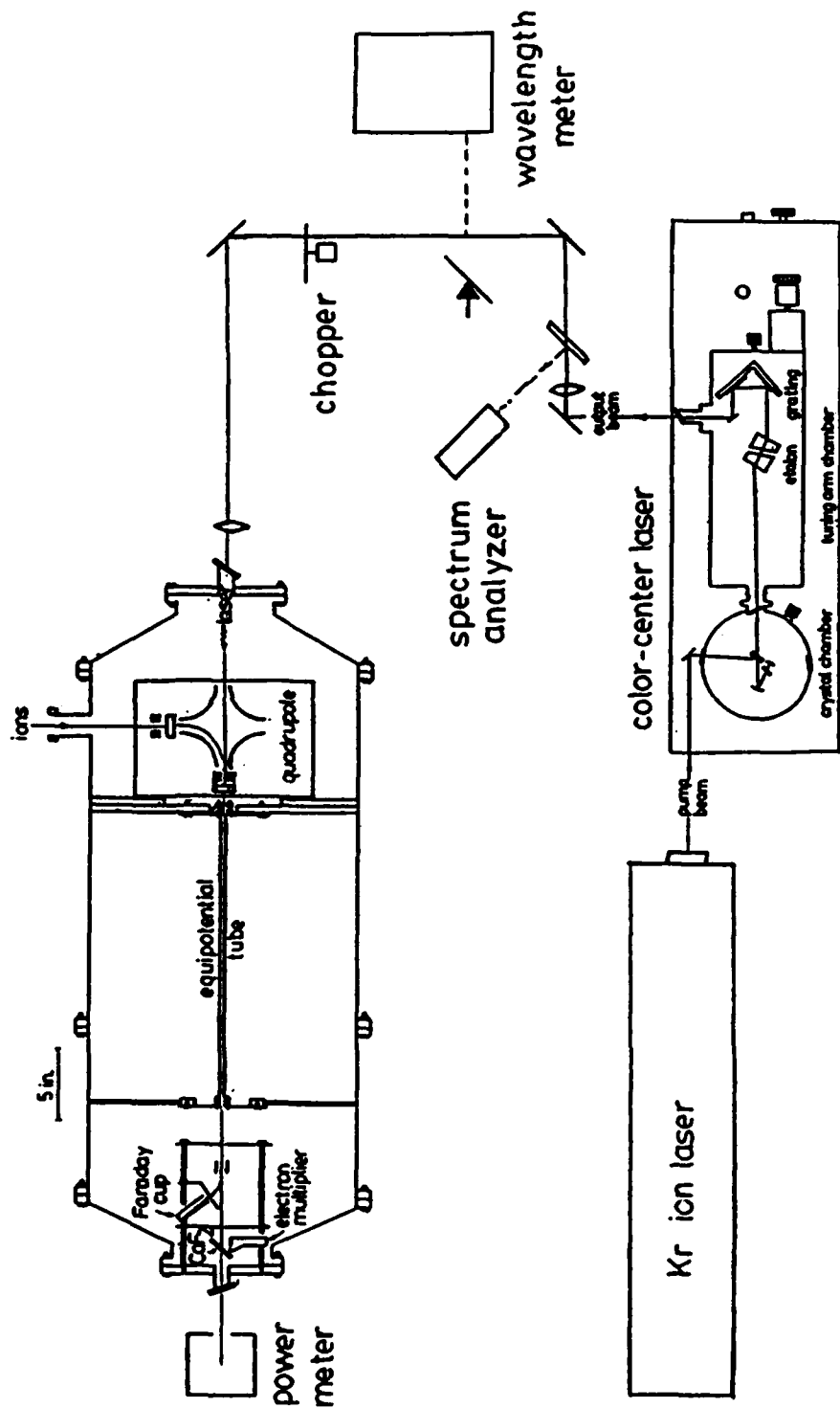


Figure 3. Fast ion beam system, showing the coaxial interaction region, detector, quadrupole ion beam bender, and IR color center laser. Ions in the interaction region are typically moving with 3000 eV.

approximately equal magnitude and opposite polarity is applied to adjacent pole pieces. Quadrupole voltages of around ± 1 kV are required to bend a 2 keV ion beam. Since the quadrupole deflects in the horizontal plane, it is used along with the vertical deflectors before and after it to direct the ion beam through the rest of the apparatus.

Ions emerging from the quadrupole assembly pass through the an einzel lens and are directed through a 1 mm aperture into a 50 cm long, $\frac{1}{4}$ inch O.D., $\frac{3}{16}$ inch I.D. stainless steel tube. The variable voltage on this "equipotential tube" changes the speed of the ions as they enter it. The ions drift through the tube at a constant speed determined by the potential of the tube when they entered it. The tube is narrow and long enough so that the potential inside is uniform except very near the ends where the ions are accelerated or decelerated. There are 1.5 mm apertures nearly touching each end of the tube that define the line along which the laser and ion beam will overlap. The beams can be focused so that about 35% of the laser power and about 80% of the ion current pass through both apertures.

The Doppler shifted frequency ν_{ion} of the laser light seen by negative ions in the equipotential tube is related to the fixed laboratory frame laser frequency ν_{lab} by

$$\nu_{ion} = \nu_{lab} \frac{1 \pm v}{(1 - v^2)^{1/2}}$$

where

$$v = \left(\frac{2e|V_a - V_t|}{Mc^2} \right)^{1/2}$$

v_a and v_t are the voltages on the anode plate and the equipotential tube, respectively. M and e are the negative ion mass and charge, respectively. v is in units of the speed of light, c . The positive (negative) sign is for anti-parallel (parallel) laser and ion beam momentum vectors. In these experiments we use the parallel geometry.

After the ions exit the equipotential tube and return to their original kinetic energy, they enter the detection assembly which is mounted on a flange at the end of the interaction region. The ions pass through a strong parallel plate deflector that directs them off the line determined by the apertures and into a Faraday cup. The cup is narrow and deep so that it is unlikely that the ions will bounce out once they have gone in. A grounded shield with a 3 mm slit covers the entrance to the cup to ensure that the beam is aimed properly. The ion current deposited into the Faraday cup is monitored by an electrometer. All lenses and deflectors in the ion beam machine are used to maximize the negative ion current making it through the tube and into the Faraday cup.

A 2 keV neutral particle, formed from a negative ion stripped of its charge after exiting the electrostatic quadrupole, is not deflected into the Faraday cup. It continues forward and energetically collides with a CaF_2 plate, causing secondary electrons to be thrown from the surface. CaF_2 is used here, and in the Brewster angle laser windows on both ends of the interaction region, because it is highly transparent over wavelengths accessible to the color-center laser. It is important that the plate is transparent so that the laser beam can continue out the end of the apparatus. The laser power making it through the apparatus is used to judge the laser alignment and to normalize measured signal strengths. The stainless steel mount holding the CaF_2 plate is charged to a potential of -2000 V. The secondary electrons ejected from the plate are accelerated toward the first dynode of a Vacuumetrics model AEM-1000 electron multiplier. The first dynode is held at -1650 V. The electron signal cascades up the dynode chain to ground where it is coupled out of the apparatus and converted to a voltage by an electrometer.

Even at a few $\times 10^{-9}$ Torr, a large contribution to the background neutral signal comes from collisional detachment. When the photon energy is greater than the binding energy of the most weakly bound electron in the negative ion, then photodetachment can

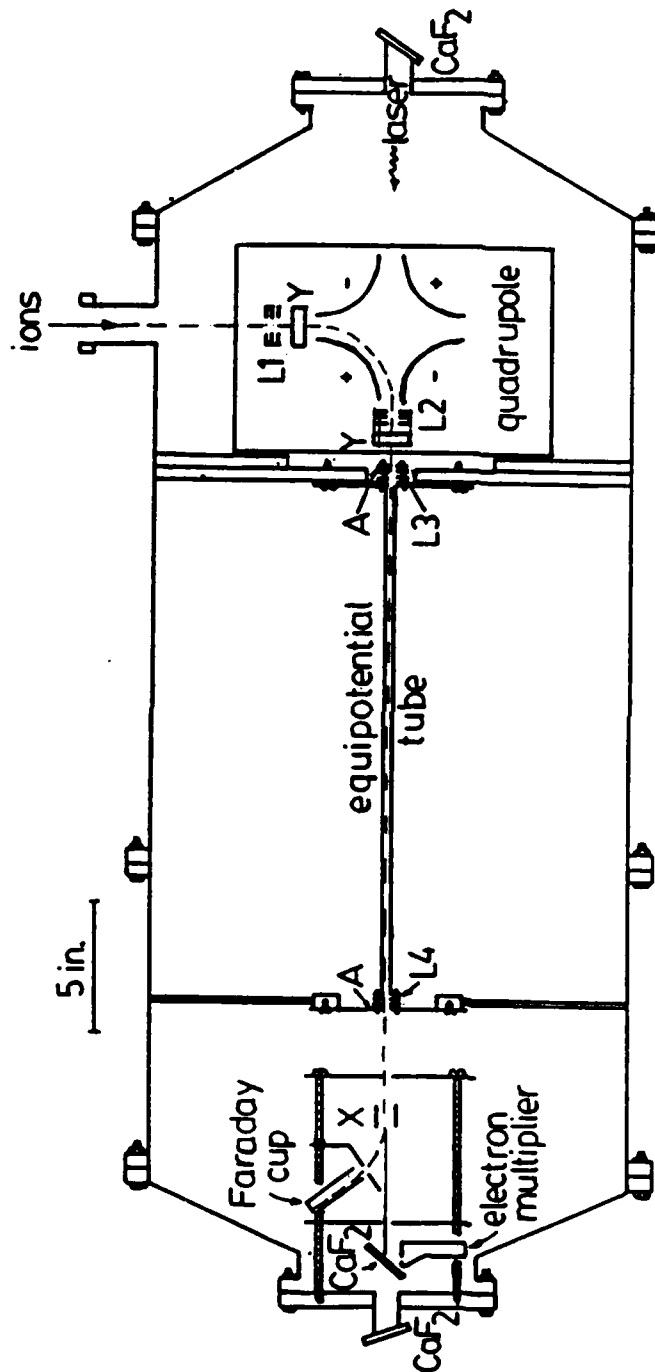


FIGURE 4. The interaction region. L1-L4 are ion lenses. X and Y are horizontal and vertical deflectors, respectively. The A's are apertures attached to current sensors.

occur. If the photon energy is also resonant with a transition in the negative ion then the electron may autodeattach before it is deflected into the Faraday cup. The resonances observed in autodeattach negative ions appear as sharp increases in the production of neutrals as the photon energy is scanned. The widths of the resonances provide a measure of the autodeattach state lifetimes. The relative strengths of the neutral signals are normalized to the laser power, ion current, and photon frequency to calculate the line intensities.

Slow Coaxial Molecular Ion Beam

The heart of the slow, molecular beam type experiment is shown schematically in Figure 5. The interest in performing the experiment in this manner is to permit the coupling of pulsed laser sources with the ion beam.

Normally, in ion beams traveling at 300-3000 eV, the densities in the beams are quite low. In order to have some possibility of having some ions in the path of the laser during a pulse, a coaxial geometry helps, as does a long interaction path. However, the laser and ion beams cannot be focused to tight waists over arbitrarily long distances, so that at some length of interaction region, diminishing returns are reached. This, plus cost, precludes the arbitrary extension of the interaction region. This problem could be helped if the ions were traveling slowly.

Because of space charge, slow ion beams are very difficult to make. However, slow ions are confined quite successfully in flowing afterglows where a neutralized plasma may be obtained.

Our design here capitalizes upon the high ion densities present in a neutralized plasma by not actually forming an ion beam but, instead, skimming out of a cold molecular expansion a molecular beam of neutrals, ions, and electrons. This plasma beam is traveling, not at hundreds of eV's worth of kinetic energy, but at hundredths of eV's kinetic energy. Ion densities are correspondingly increased.

Mass detection is achieved with a time-of-flight mass spectrometer subsequent to wavelength selective photodestruction by the laser pulse. A simple laser-on minus laser-off differencing scheme produces the signal corresponding to disappearance of the ions. With this type of apparatus, all O^- emanating from the source and present in the interaction region can be destroyed with each pulse of a 3 mJ green laser. This sensitivity allows detection of cross sections down to 10^{-20} cm^2 .

Source Development

Three types of ion sources were used in producing ions: the Branscomb source, the Bowen source, and the CESE source. The first of these is most suited for stable negative ions with rather high electron affinities and produces ions with approximately room temperature rotational temperatures. The latter two sources utilize supersonic expansions to produce rotationally cold ions, and fragile cluster ions.

Branscomb-type Source

Figure 6 shows a uniplasmatron-like Branscomb source used in forming the HNO^- ions [36]. This source is a hot filament type, with about 0.1 to 1 torr of gas behind a 1 mm extraction aperture. Unfortunately, this standard negative ion source has not proven useful in generating the other, more fragile negative ions under study here, and more elaborate sources must be used.

Bowen-type Source

The Bowen [5] source supplants the Branscomb source when the preparation of

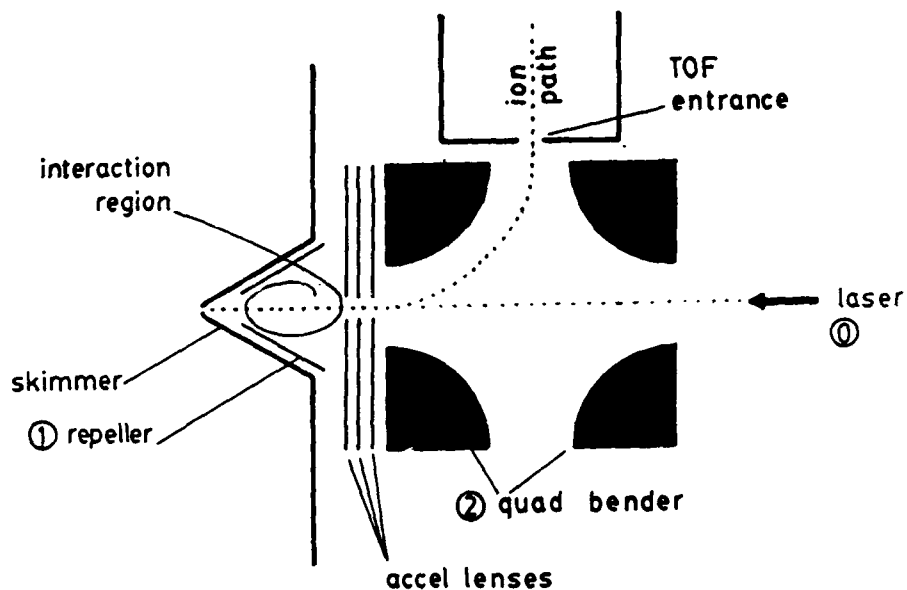


Figure 5. Coaxial interaction region of the slow molecular ion beam, and adjacent skimmer, repeller, and quadrupole beam bender for separation of ions from the plasma and ion injection into the time-of-flight mass spectrometer. Note the scale: the interaction region proper is only about 1 cm in length. Typically ions are moving less than 0.1 eV in the interaction region.

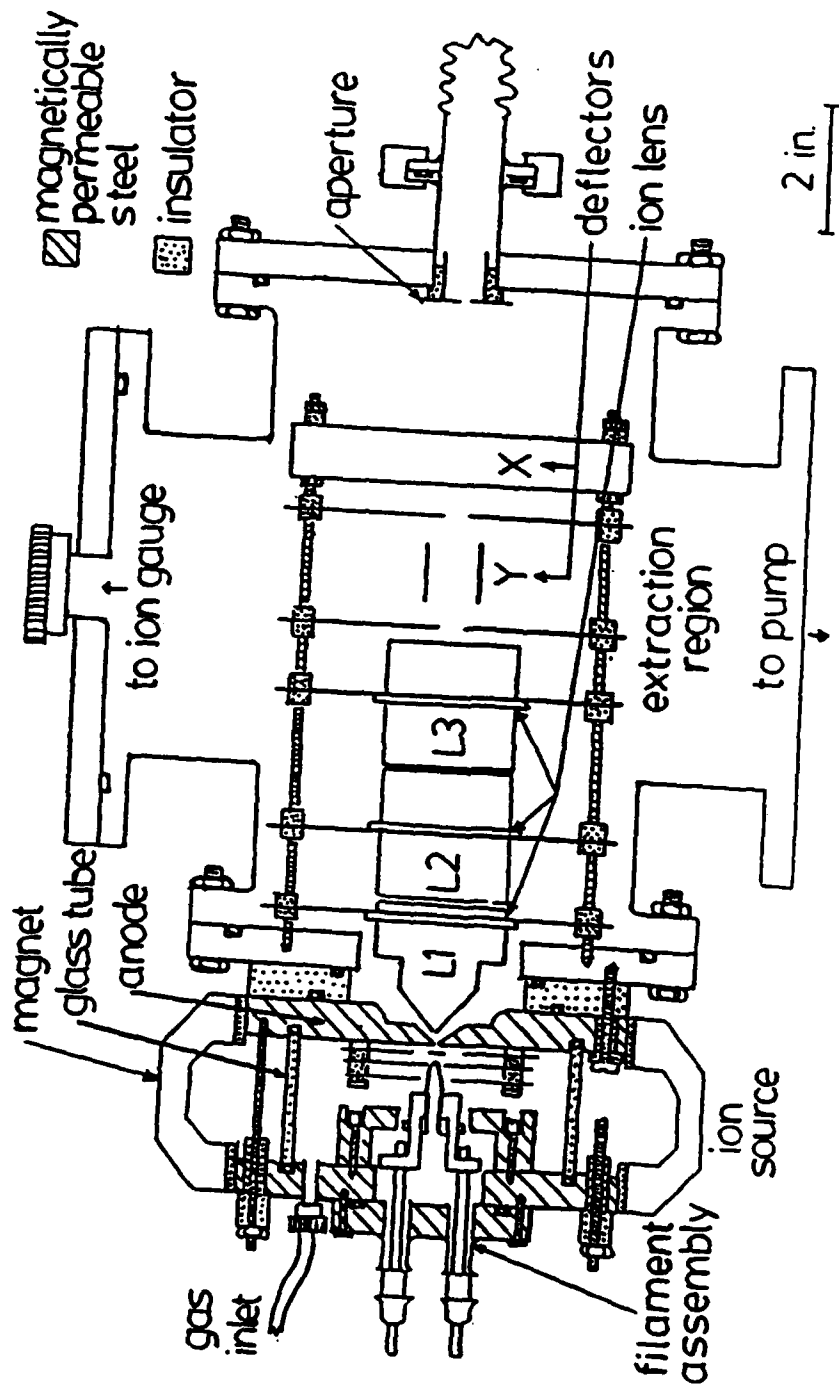


Figure 6. Branscomb-type ion source, showing adjacent extraction ion optics. Typical operating pressures are 0.1 to 1 torr of gas in the ion source.

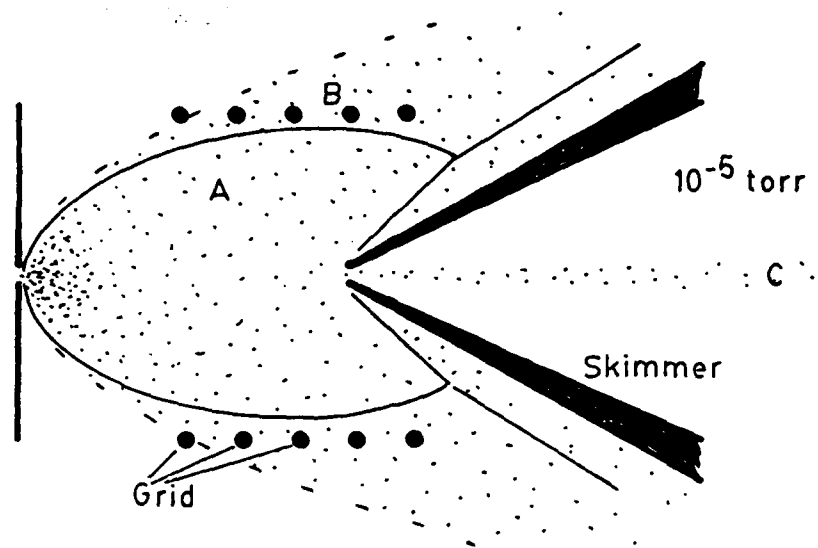


Figure 7. Operation of the skimmer in a high-pressure nozzle source. The pressure behind the nozzle is typically 1-4 atm. Three regions are shown: (A) the free expansion within the shock envelope, (B) the boundary flow outside the barrel shock, and (c) the skimmed, cold plasma beam. The function of the grid electrode is to control the plasma-skimmer potential difference, to allow ions to pass unhindered through the skimmer aperture. Excitation in this case is depicted as that of the CESE, with a corona electrode shown in place behind the high pressure nozzle.

more fragile species is desired. It is based upon the original work of Haberland [37]. In it, gas issues from a nozzle into a high vacuum region. This passes through a region of electron impact where negative ions are formed.

Corona-Excited Supersonic Expansion

The Corona-Excited Supersonic Expansion is modified from that used successfully in the preparation of radicals in molecular beams [38]. Like the Bowen source, the heart is a supersonic gas expansion. This source differs from the Bowen source in that the ions are formed not by electron impact, but instead by corona discharge on the high pressure side of the nozzle. In this source, ionization occurs before expansion.

Low velocity molecular beams are extracted by skimming this expansion plasma, as shown in Fig. 7.

Cooling attainable with this type of nozzle source was investigated by Andreas Ante, as reported in his thesis [39].

Results

Results have been achieved in several areas. One of the molecular ions studied yielded a wealth of data; the others proved more difficult to produce in quantities that would permit detailed spectroscopic investigation.

Molecules

HNO⁻

The infrared spectrum of the nitroxide ion, HNO⁻, has been recorded in the region between 2940 and 3050 cm⁻¹ using high resolution autodetachment detection spectroscopy. This wave number range corresponds to absorption near the ν_1 vibration, the N-H stretching mode. The rR4, rR5, rR6, rR7, rR8, rR9, and rQ7 branches have been identified and rotationally analyzed, and rotational and centrifugal distortion constants for the (0,0,0) and (1,0,0) states have been obtained. The principal rotational constants, in cm⁻¹, are: $A'' = 15.233360(380)$; $(B'' + C'')/2 = 1.096829(24)$; $(B'' - C'')/2 = 0.034424(900)$; $A' = 16.937355(280)$; $(B' + C')/2 = 1.088597(22)$; $(B' - C')/2 = 0.036066(1600)$. The ν_1 band origin is 2750.7827(53) cm⁻¹. Details of this experiment have been reported elsewhere [36,40], only a summary is given here.

HNO⁻ was prepared in a Branscomb-type ion source (Figure 6) from ethyl nitrite. The resulting beam was admitted into the velocity tuned interaction region of the fast ion beam, and was probed by IR from an F-center laser (Figure 3). The ions surviving the encounter were swept into a Faraday cup where their current was monitored. The ions which absorbed radiation and detached gave rise to energetic neutrals, detected by the secondary electrons ejected from a CaF window. These electrons were amplified by a particle multiplier, and comprised the signal that was monitored as a function of laser wavelength and ion velocity.

The relevant energy levels are shown in Figure 8. Promotions from the (0,0,0) ground vibrational state into the (1,0,0) vibrational state of HNO⁻ are shown on the left. Nearby in energy (on the right of the figure) are the levels corresponding to the ground vibrational state of the HNO neutral itself, permitting autodetachment to proceed. This permits observation of sharp, structured absorption in the ion at IR wavelengths, but also allows the detection by neutral production through the process of slow autodetachment. The resulting spectrum is shown schematically in Figure 9, which is a compilation of hundreds of individual laser and velocity tuned spectral regions. These do not show the individual K-type doubling that was observed on most lines. Individual line positions

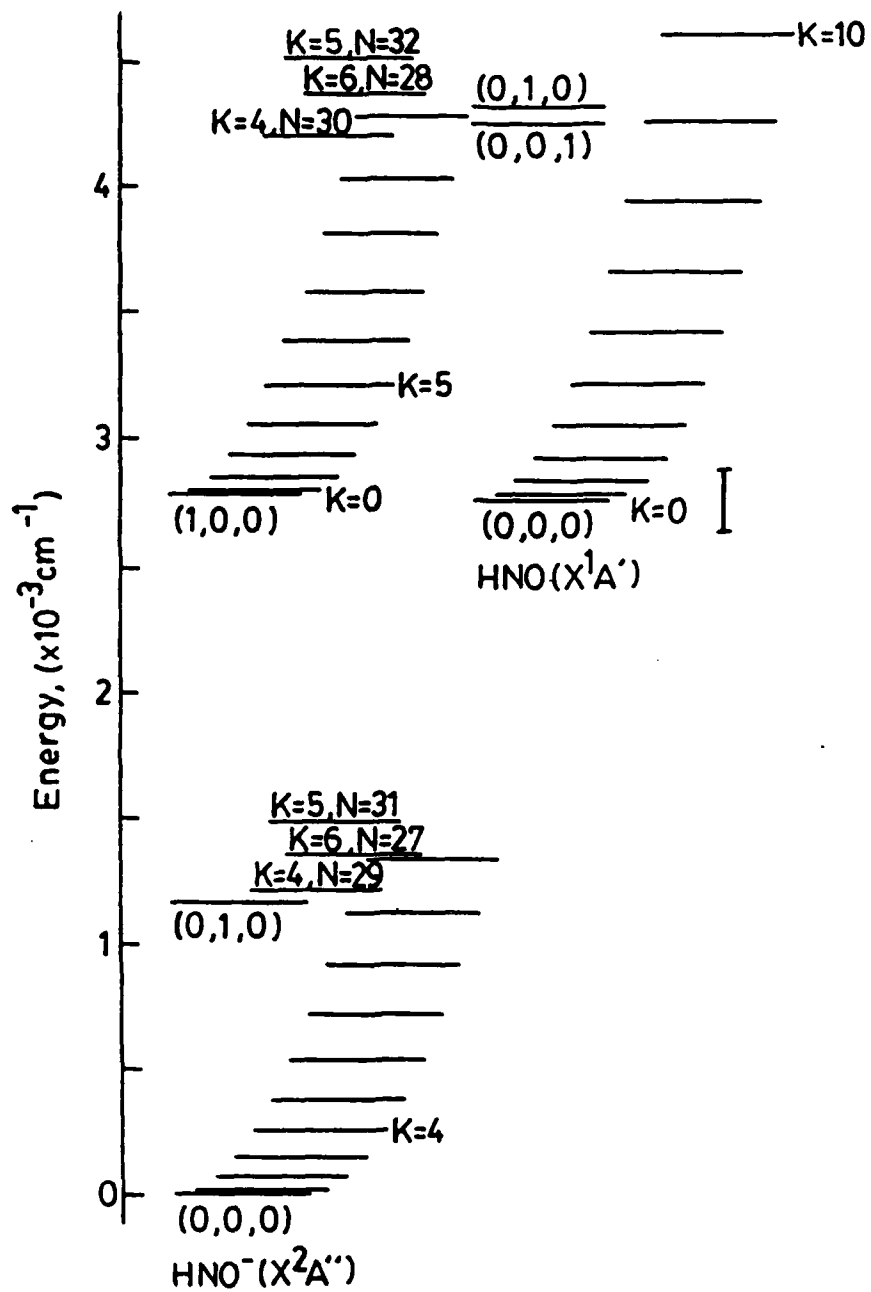


Figure 8. Energy levels of HNO^- (left) and HNO (right).

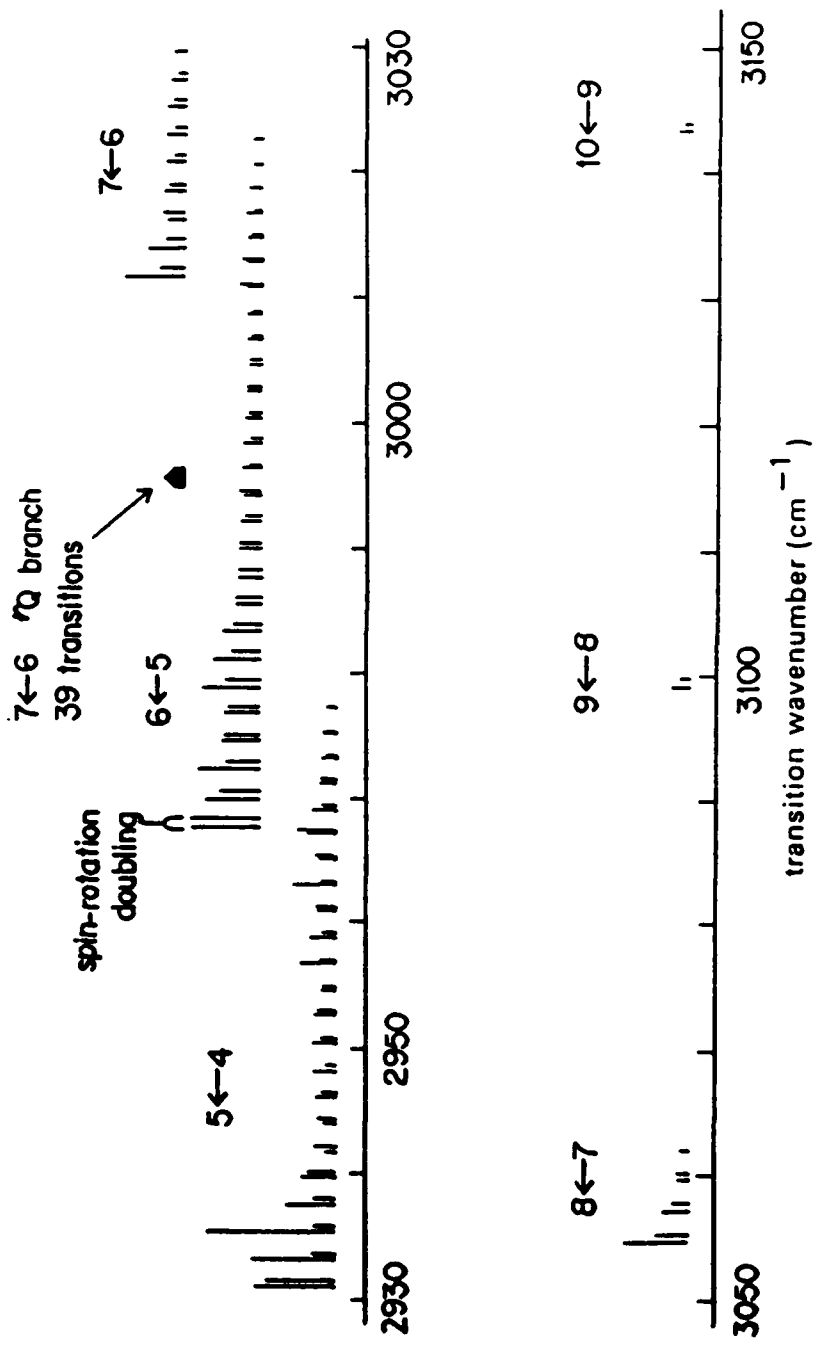


Figure 9. Transitions observed in the spectrum of HNO^- .

have been tabulated elsewhere [36,40].

One aspect of the data obtained with high resolution is shown in Figure 10. Individual lines acquire line widths as a result of the autodetachment lifetimes of individual states. The lifetimes are in the range of 3-15 nanoseconds, and vary with quantum numbers. The details of these dependences are not understood yet theoretically, and correspond to an open question for investigation. The pattern is much more complicated than for NH^- autodetachment, where the rates are explained by a picture of the breakdown of the Born-Oppenheimer separation in this molecular ion [41].

The set of molecular constants obtained from the fit to the data is shown in Table I, according to the effective Hamiltonian defined explicitly in Table II [42,43].

The rotational inertia constants place a significant constraint upon the geometry of the HNO^- ion. This is depicted graphically in Figure 11. Both the H-N and N-O bonds are anomalously long. The region of agreement of these geometry constraints and the N-O bond length found by Ellis and Ellison [11] from a Franck-Condon fit of vibrational progressions (open circles) indicates an HNO bond angle of about 110 degrees. Accordingly, the H-N bond becomes 1.18 Angstroms. Definitely, the bonding in this species is quite unusual for the atoms involved, compared with that in familiar compounds [44].

NH_4^-

The possibility of finding the high energy form of the ammonium anion was given impetus by the discovery of emissions from the neutral NH_4 radical in cold nozzle expansions, both in our labs and elsewhere [45]. These radicals are the analogues of the metastable Rydberg ions we are searching for here, except that they have one extra electron, located in an outer Rydberg orbital surrounding a central ammonium ion core, instead of the two electrons in the anions. Thus, we have confirmation that the appropriate excited Rydberg states are being formed.

The ammonium anion NH_4^- has proven to be difficult to prepare in abundance. This ion is not obtained in the Branscomb-type source. It is found to occur weakly, under clustering conditions, in nozzle expansion sources of the Bowen and CESE type. Figure 12 shows the mass spectrum obtained.

The beams were too tenuous to allow spectral scans of this ion in a manner similar to that used successfully in the study of HNO^- , as above. (For a comparison, the maximum amounts of NH_4^- formed correspond to less than a picoampere, while the experiments on HNO^- were performed with about 2 nanoamperes--three orders of magnitude weaker.) Instead, only fixed frequency detachments were attempted in both the green and near IR portions of the spectrum, near 1000 and 500 nm. No depletion of the beam was observed with the IR, but the ions disappeared under visible irradiation. The intensity used was sufficient to make 80% of O^- ion calibrant disappear; the resulting cross section of NH_4^- to photodestruction by green light is estimated near 10^{-18} cm^2 .

CH_5^-

Attempts to make the related carbon-centered anion failed. It is not known whether this ion is difficult to prepare, or does not exist on microsecond time scales.

During these attempts, a variety of other scientifically interesting carbon-containing ions were produced, including C_3^- , one of the first polyatomic ions to be photodetached. Interestingly, attempts to detach this ion failed. Subsequently, the reason for this failure turned out to be the very cold vibrational distributions produced by the sources in use; the earlier detachments were attempted from vibrationally excited levels. This evidence points to excellent cooling conditions in the source used, which would have favored formation of very fragile species. Indeed, some of these polycarbon species evidenced unusually high numbers of hydrogens (e.g., C_2H_7) in their mass spectra, and it may be that hypervalent polycarbon ions were present, in addition to just weakly bound ionic clusters. Some of

Table I Effective rotational constants for the ν_1 band of HNO^- .

Constant	Value (cm^{-1}) ^a	
	(0,0,0)	(1,0,0)
T	-	2750.782650(5300)
A	15.233360(380)	16.937355(280)
$\frac{1}{2}(B+C)$	1.096829(24)	1.088597(22)
$\frac{1}{2}(B-C)$	0.034424(900)	0.036066(1600)
Δ_N ($\times 10^6$)	4.6838(340)	6.7478(300)
Δ_{NK} ($\times 10^3$)	-2.16615(100)	-1.64593(66)
Δ_K ($\times 10^2$)	2.1060(10)	2.1055(6)
Φ_N ($\times 10^9$)	4.123(40)	4.290(30)
Φ_{KN} ($\times 10^5$)	-2.7891(25)	-1.2920(16)
$\epsilon_{aa} - \frac{1}{2}(\epsilon_{bb} + \epsilon_{cc})^b$	-0.454287(3600)	-0.500069(2200)
$\frac{1}{2}(\epsilon_{bb} + \epsilon_{cc})^b$ ($\times 10^3$)	3.157(1600)	2.4140(1600)
Δ_K^S ($\times 10^4$) ^b	9.4253(6400)	9.4253 ^c

^a Errors quoted in parentheses are one standard deviation in units of the last significant figure of the constant.

^b The spin-rotation constants were frozen at values returned from the fit to the spin-rotation splittings. The quoted errors are from the spin-rotation fit.

^c Constrained to the (0,0,0) value.

Table II. Matrix elements of the A reduced effective rotational and spin-rotation Hamiltonian.

$$\begin{aligned} \langle N, K | \mathcal{H}_{\text{rot}} | N, K \rangle &= AK^2 + \frac{1}{2}(B+C)(N(N+1) - K^2) - \Delta_N^S N^2 (N+1)^2 \\ &\quad - \Delta_{NK}^S N(N+1)K^2 - \Delta_K^S K^4 + \Phi_N^S N^3 (N+1)^3 + \Phi_{NK}^S N^2 (N+1)^2 K^2 \\ &\quad + \Phi_{KN}^S N(N+1)K^4 + \Phi_K^S K^6 \end{aligned}$$

$$\begin{aligned} \langle N, K \pm 2 | \mathcal{H}_{\text{rot}} | N, K \rangle &= (\frac{1}{4}(B-C) - \delta_N^S N(N+1) - \frac{1}{2}\delta_K^S ((K \pm 2)^2 + K^2)) \\ &\quad + \phi_N^S N^2 (N+1)^2 + \frac{1}{2}\phi_{NK}^S N(N+1)((K \pm 2) + K^2) + \frac{1}{2}\phi_K^S ((K \pm 2)^4 + K^4) \\ &\quad \cdot ([N(N+1) - K(K \pm 1)][N(N+1) - (K \pm 1)(K \pm 2)])^{\frac{1}{2}} \end{aligned}$$

$$\begin{aligned} \langle N, K | \mathcal{H}_{S-R} | N, K \rangle &= f(J, N) [\epsilon_{aa} K^2 + \frac{1}{2}(\epsilon_{bb} + \epsilon_{cc})(N(N+1) - K^2) \\ &\quad + \Delta_K^S K^4 + (\Delta_{NK}^S + \Delta_{KN}^S) K^2 N(N+1) + \Delta_N^S N^2 (N+1)^2] \end{aligned}$$

$$\begin{aligned} \langle N, K | \mathcal{H}_{S-R} | N-1, K \rangle &= -[\epsilon_{aa} - \frac{1}{2}(\epsilon_{bb} + \epsilon_{cc}) + \Delta_K^S K^2 \\ &\quad + \Delta_{NK}^S N^2] [K/2N] [N^2 - K^2]^{\frac{1}{2}} \end{aligned}$$

$$\begin{aligned} \langle N, K | \mathcal{H}_{S-R} | N, K \pm 2 \rangle &= f(J, N) [\frac{1}{4}(\epsilon_{bb} - \epsilon_{cc}) + \delta_N^S N(N+1) \\ &\quad + \frac{1}{2}\delta_K^S (K^2 + (K \pm 2)^2)] \\ &\quad \cdot ([N(N+1) - K(K \pm 1)][N(N+1) - (K \pm 1)(K \pm 2)])^{\frac{1}{2}} \end{aligned}$$

$$\begin{aligned} \langle N, K | \mathcal{H}_{S-R} | N-1, K \pm 2 \rangle &= -[1/4N] [\frac{1}{2}(\epsilon_{bb} - \epsilon_{cc}) + \delta_N^S (K(N \pm K) + (K \pm 2)(N \pm K + 2))] \\ &\quad \cdot [(N \mp K - 1)(N \pm K + 1)(N \mp K - 2)(N \mp K)]^{\frac{1}{2}} \end{aligned}$$

$$\begin{aligned} f(J, N) &= [2(N+1)]^{-1} & (J=N+\frac{1}{2}) \\ &= -[2N]^{-1} & (J=N-\frac{1}{2}) \end{aligned}$$

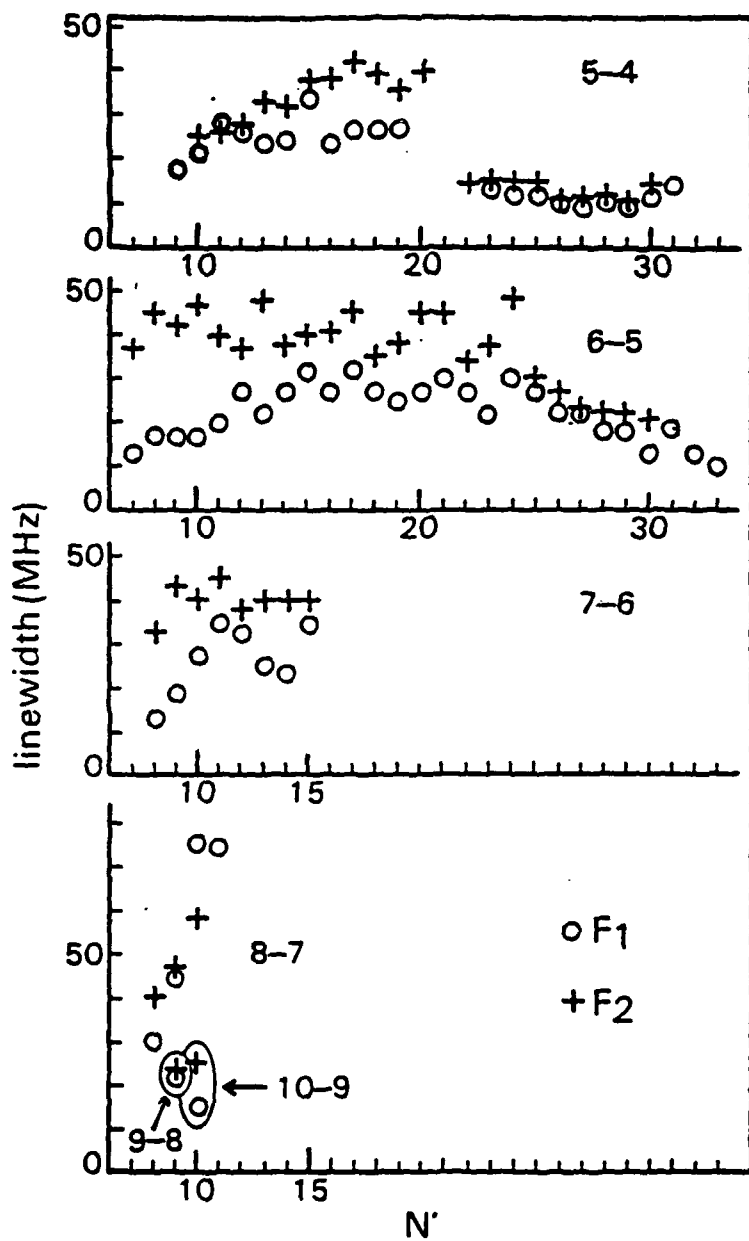


Figure 10. Linewidths observed as a function of quantum level, caused by dissociative rate broadening.

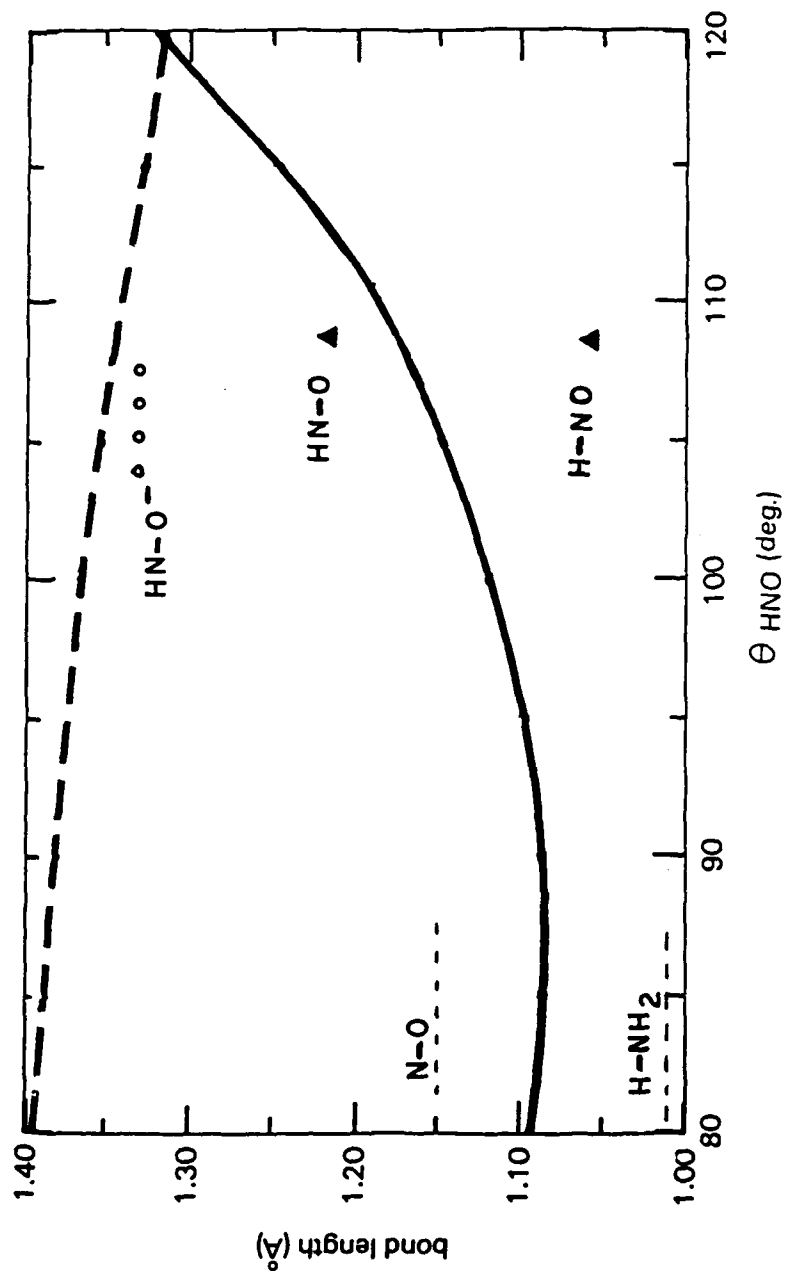


Figure 11. Permissible HNO^- geometries: bond lengths vs. bond angles. Upper dotted curve shows the N-O bond length; the lower solid curve corresponds to the H-N bond. Comparison data is shown for the molecules NO, NH_3 , and the neutral HNO .

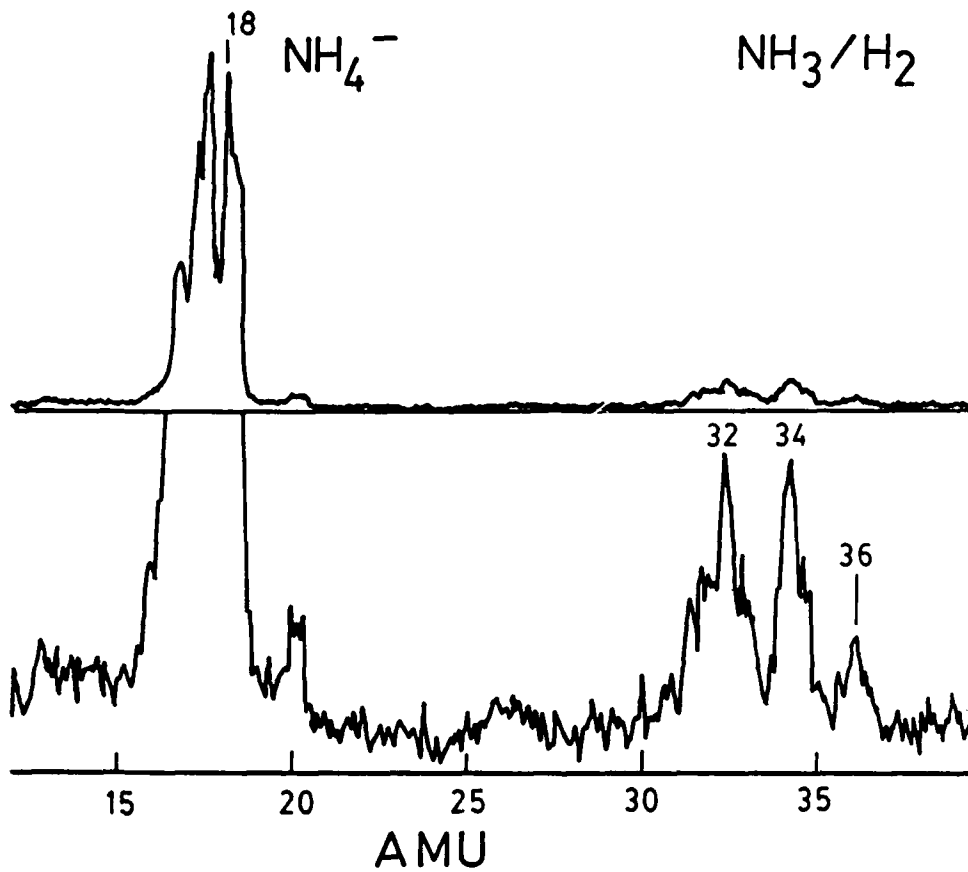


Figure 12. Mass spectrum showing the NH_4^- anion (mass 18) prepared in a nozzle expansion of H_2 and ammonia.

these ions were found to photodetach or photodissociate with visible radiation. This may be an area of further interest.

SiH₅⁻

Experimental difficulties in the work with silanes caused extensive down-time after only a few hours of operation, as silicon had to be removed from every surface of the source. Because of the tight time schedule, the silicon studies were deferred to a renewal period where sufficient time could give them justice. Experience with HNO₃⁻, NH₄⁻ and CH₅⁻ had shown that extreme care, time and patience was required to establish the condition of their preparation. The concern here was that a significant advance may be missed and that a hasty negative result would be misleading. Because of much slower progress with silicon ion sources, the remaining time was deemed inadequate to establish if it were the desirable, high energy, form. Instead, more time was devoted to the CH₅⁻ anion search.

Other Technical Advances

Photodissociation

One mechanism for photodissociation is that of energy randomization within an ion, leading to "evaporation" of a fragment. This model was tested by applying the theoretical predictions against N₂⁺ dissociation [46]. Good agreement was found in the ability of the model to explain the data, giving encouragement to the application of such a model to anion photodestruction. This model has now been used by a number of other groups working in ion photodestruction. It has been used successfully to obtain the binding energies of fragments within an ion.

Photodetachment

Because one of the methods by which hypervalent species could be distinguished from just hydride cluster ions is in the location and shape of the photodetachment cross section as a function of energy, more careful analysis of the range of validity of threshold law scaling was made [47].

It was found that a simple one-electron analysis was quite helpful, the so-called zero-core-contribution (ZCC). This approximation could be used to find analytic expressions for detachment processes that could be compared to the more heuristic Wigner threshold scaling relations. This method is applicable to molecules, such as studied here, when the photodetachment is direct and there are no long-range polarization forces. Not too surprisingly, the Wigner approximation had a very limited range of accuracy, while the ZCC picture afforded an understanding of the cross section as much as a volt above threshold.

Experimental Techniques

In addition to the design and construction of a novel molecular ion beam apparatus, progress was made in the area of ion sources. The CESE had never been used for ion production in a beam machine; it has now been shown that such a design gives results that are comparable to sources based upon electron impact on molecular expansions. It has also been determined that skimming of such a plasma is possible if careful attention is paid to the relative plasma-skimmer potential.

Even with careful skimming, the plasma beam extracted from such an expansion has an instability that can lead to ion losses if the beam is not contained by forces corresponding to the order 10 eV potentials. The mechanism for beam instability was eventually determined to be that of supra-elastic collisions of electrons with excited metastable

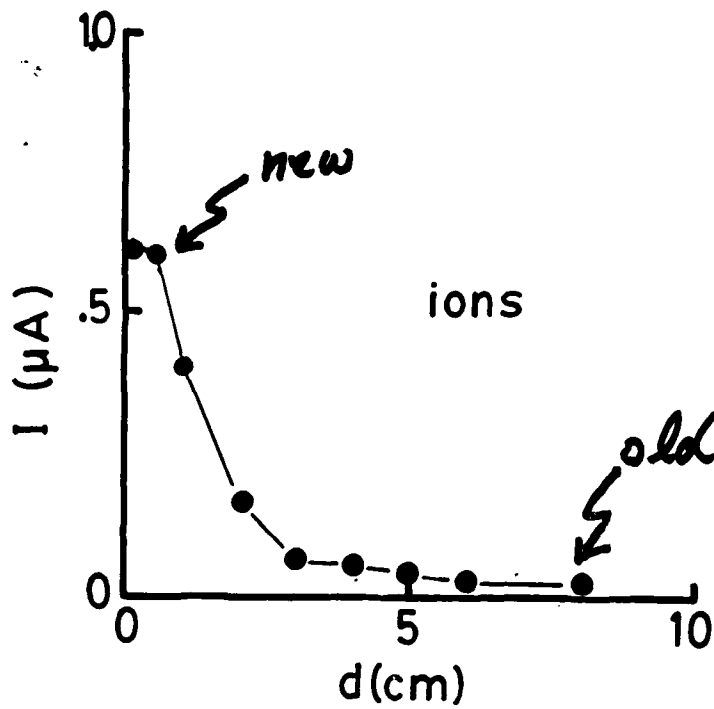


Figure 13. Ions found on axis in skimmed plasma beam, as a function of distance from skimmer, d . Comparison of older and newer design points is shown.

neutrals in the plasma. These electrons are first ejected from the plasma with approximately 10-20 eV worth of energy. The resulting positive space-charge build-up in the plasma leads to radial expansion that is initiated about a centimeter after the plasma is skimmed into a beam. Subsequently, for a 1 mm diameter beam, ions on the beam axis fall to a third of their initial density within 2 cm (Figure 13).

This mechanism caught us by surprise, and it took us some time to understand the cause. In the end, the problem was addressed by a redesign of the interaction region, moving it to within a centimeter of the position of beam skimming. This gave easily an increase of a factor of 30 in ion density on axis, and permitted much better overlap of the laser and ion beam columns.

The result is that we now understand how to skim a Mach 100, supersonic plasma.

Conclusions

The possibility of finding high energy anions, based upon the metastability of a hypervalent species, was investigated. One anion, HNO^- , was investigated in detail. Other anions were found to be difficult to prepare, and only limited information on these was obtained. It is believed that NH_4^- high energy form has been observed, while there was no evidence for the formation of the CH_5^- ion. The SiH_5^- anion structure still needs to be investigated spectroscopically.

Two methods of understanding the dissociation and detachment of molecular ions were developed to handle these processes.

The ability to form a skimmed, molecular ion beam from a Mach 100 nozzle expansion was developed in the course of these studies.

Publications

J.W. Farley, Phys. Rev. A, 40, 6286 (1989)

"Photodetachment Cross Sections of Negative Ions: The Range of Validity of the Wigner Threshold Law."

P.C. Engelking, Chem. Phys. Lett. 139, 6 (1987)

"'Magic' Losses from Metastable N_{2n}^+ Clusters as a Statistical Evaporation Process."

H.C. Miller, J.L. Hardwick, and J.W. Farley, J. Mol. Spec. 134, 329 (1988)

"The Vibration-Rotation Spectrum of the ν_1 Band of Nitroxide HNO^- ."

THESES

Autodetachment Spectroscopy of the Imide and Nitroxide Anions.

Harold C. Miller, (Univ. of Oregon, June 1988).

Development of a Supersonic Nozzle System to Produce Cluster Ions.

Andreas Ante (Univ. of Aachen, March 1989).

References

- [1] "An *ab-initio* study of the tetrahedral NH_4^- ion." H. Cardy, C. Larrieu, and A. Dargelos, *Chem. Phys. Lett.* **131**, 507 (1986).
- [2] "Vertical and adiabatic ionization energies of NH_4^- isomers via electron propagator theory and many body perturbation theory calculations with large basis sets." J. V. Ortiz, *J. Chem. Phys.* **87**, 3557 (1987).
- [3] "Theoretical determination of molecular structure and conformation. 17. On the existence of FH_2^- , OH_2^- , NH_2^- , and CH_2^- in the gas phase." D. Cremer and E. Kraka, *J. Phys. Chem.* **90**, 33 (1986).
- [4] "'Double-Rydberg' molecular anions." M. Gutowski, J. Simons, R. Hernandez, and H. L. Taylor, *J. Phys. Chem.* **92**, 6179 (1988).
- [5] "Negative ion photoelectron spectroscopy of the negative cluster ion, $\text{H}^-(\text{NH}_3)_n$," J. V. Coe, J. T. Snodgrass, C. B. Freidhoff, K. N. McHugh, and K. H. Bowen, *J. Chem. Phys.* **83**, 3169 (1985).
- [6] "Collision-induced dissociation and charge reversal experiments on H_2O^- and NH_4^- ." W. DeLange and N. M. Nibberling, *Int. J. Mass Spectr. Ion Phys.* **80**, 201 (1987).
- [7] "Theoretical studies of proton-transfer reactions. III. The reactions of hydride ions with ammonia and methane." C. D. Ritchie and H. F. King, *J. Am. Chem. Soc.* **90**, 838 (1968).
- [8] "On the H^- migration in the NH_4^- ion." J. Kalcher, P. Rosmus, and M. Quack, *Can. J. Phys.* **62**, 1323 (1984).
- [9] "Pathways for Nucleophilic substitution at silicon. A molecular orbital approach." J. A. Deiters and R. R. Holmes, *J. Am. Chem. Soc.* **109**, 1692 (1987).
- [10] "NBS tables of chemical thermodynamic properties -- selections for inorganic and C, and C₂ organic substances in SI units." D. D. Wagman, et al., *J. Phys. and Chem. Ref. Data.* **11**, Sup. 2 (1982).
- [11] "Photoelectron spectroscopy of HNO^- and DNO^- ." H. B. Ellis and G. B. Ellison, *J. Chem. Phys.* **78**, 6541 (1983).
- [12] "The infrared spectrum of HNO ." J. W. C. Johns, A. R. McKellar, and E. Weinberger, *Can. J. Phys.* **61**, 1106 (1983).
- [13] "Formation of NH_4^- ion in the gas phase." J. C. Kleingeld, S. Ingemann, J. E. Jalonen, and N. M. M. Nibbering, *J. Am. Chem. Soc.* **105**, 2474 (1983).
- [14] "Chemical equilibrium of $\text{NH}_2^- + \text{H}_2 \rightleftharpoons \text{H}^- + \text{NH}_2^-$ and the determination of $D_0^\circ(\text{NH}_2-\text{H})$." R. S. Hemsworth and R. W. Rundle, *J. Chem. Phys.* **59**, 77 (1973).
- [15] "Hypervalent silicon hydrides: SiH_5^- ." D. J. Hadjasz and R. R. Squires, *J. Am. Chem. Soc.* **108**, 3139 (1986).
- [16] "The reactions between negative hydrogen ions and silane." U. Brandemark and P. E. Siegbahn, *Th. Chem. Acta* **66**, 233 (1984).

- [17] "The molecular orbital description of SN2 reactions at silicon centers." P. Baybutt, *Mol. Phys.* **29**, 389 (1975).
- [18] "Quantum-chemical investigation of the silicon and carbon coordination bond in their isostructural compounds." N. M. Vitkovskaya, V. B. Mantsivoda, T. E. Moskovskaya, and M. G. Voronkov, *Int. J. Quantum Chem.* **17**, 299 (1980); "Quantum chemical analysis of silicon atom pentacoordination." Y. L. Frolov, S. G. Shevchenko and M. G. Voronkov, *J. Organometallic Chem.* **292**, 159 (1985).
- [19] "Theoretical studies of the reactions $XH_n \rightarrow XH_{n-1} + H^+$ and $XH_{n-1} + SiH_4 \rightarrow [SiH_4XH_{n-1}]^-$." M. S. Gordon, L. P. Davis, L. W. Burggraf, and R. Damrauer, *J. Am. Chem. Soc.* **108**, 7889 (1986).
- [20] "Theoretical study of the molecular ions SiH_5^+ and SiH_3^- ." F. Keil and R. Ahlrichs, *Chem. Phys.* **8**, 384 (1975).
- [21] "Electronic structure of SiH_5^+ and model studies of inter- and intramolecular exchange in pentacoordinate silicon species." D. L. Wilhite and L. Spialter, *J. Am. Chem. Soc.* **95**, 2100 (1973).
- [22] "Bildungsweise und Struktur des Pentebromocarbonat - Anions $[CBr_5]^-$ -- Zur Oxidation von Enaminen." F. Effenberger, et. al., *Chem. Ber.* **109**, 306 (1976); "Die Struktur des Anions $[CBr_5]^-$ im Kristallinen Tetraphenylphosphonium-pentabromocarbonat." H. J. Linder and B. K.-V. Gross, *Chem. Ber.* **109**, 314 (1976).
- [23] "The electronic structure of carbonium ions. Alkyl cations and protonated hydrocarbons." T. Yonezawa, H. Nakatsuji, and H. Kato, *J. Am. Chem. Soc.* **90**, 1239 (1968).
- [24] "Non-empirical LCAO MO SCF studies on CH_5^+ ." J. L. Gole, *Chem. Phys. Lett.* **3**, 577 (1969); (Corrections) **4**, 408 (1969).
- [25] "Retention and inversion in bimolecular substitution reactions of methane." W. T. Van der Lugt and P. Ros, *Chem. Phys. Lett.* **4**, 389 (1969).
- [26] "Organic quantum chemistry. XXIV. A theoretical study of the stereochemistry of SE2 and SN2 reactions." N. L. Allinger, J. C. Tai, and F. T. Wu, *J. Am. Chem. Soc.* **92**, 579 (1970).
- [27] "An *ab initio* LCGO-MO-SCF calculation of the potential energy surface for an SN2 reaction." C. D. Ritchie and G. A. Chappell, *J. Am. Chem. Soc.* **92**, 1819 (1970).
- [28] "The electronic structure and stability of CH_5^+ and CH_3^- ." J. J. Mulder and J. S. Wright, *Chem. Phys. Lett.* **5**, 445 (1970).
- [29] "Molecular orbital theory of SN2 reactions." J. P. Lowe, *J. Am. Chem. Soc.* **93**, 301 (1971).
- [30] "The intrinsic reaction coordinate. An *ab initio* calculation for $HNC \rightarrow HCN$ and $H + CH_4 \rightarrow CH_3 + H^-$." K. Ishida, K. Morokuma, A. J. Komornicki, *J. Chem. Phys.* **66**, 2153 (1977).
- [31] "A comparative study of some SN2 reactions through *ab initio* calculations." A. Dedieu and A. Veillard, *J. Am. Chem. Soc.* **94**, 6730 (1972).

- [32] "Ab initio calculations of small hydrides including electron correlation." V. Dyczmons and W. Kutzelnigg, *Theor. Chim. Acta* (Berlin) **33**, 239 (1974).
- [33] "Geometrical and electronic structure of hydrated CH_3^+ and CH_3^- ." P. Cremaschi and M. Simonetta, *Theor. Chim. Acta* (Berlin) **37**, 341 (1975).
- [34] "Determination of structure and bonding in simple carbonium ions by semiempirical molecular orbital method." C. P. Dwivedi, *Ind. J. Phys.* **58B**, 69 (1984).
- [35] "Studies on quixotic molecules: Part II - Molecular geometry, electronic structure and common properties of some hypothetical molecules belonging to AB_3 , AH_3 , AH_3 , and HAB_3 classes." G. D. Mahajan and B. M. Deb, *Ind. J. Pure and Appl. Phys.* **20**, 453 (1982).
- [36] H. C. Miller, Autodetachment Spectroscopy of the Imide and Nitroxide Anions, (Univ. of Oregon, thesis, June 1988).
- [37] "Mass spectra of negatively charged water and ammonia clusters." H. Haberland, H.-G. Schindler, and D. R. Worsnop, *Ber. Bunsenges. Phys. Chem.* **88**, 270 (1984).
- [38] "Supersonic expansion cooling of electronically excited OH radicals." A. T. Droege and P. C. Engelking, *Chem. Phys. Lett.* **96**, 316 (1983); "Corona excited supersonic expansion." P. C. Engelking, *Rev. Sci. Instrum.* **57**, 2277 (1986).
- [39] Andreas Ante, Development of a Supersonic Nozzle System to Produce Cluster Ions, (Univ. of Aachen, thesis, march 1989).
- [40] "The vibration-rotation spectrum of the ν_1 band of nitroxide, HNO^- ." H. C. Miller, J. L. Hardwick and J. W. Farley, *J. Mol. Spectr.* **134**, 329 (1988).
- [41] "Measurement of hyperfine structure in the infrared rotation-vibration spectrum of NH^- ." H. C. Miller and J. W. Farley, *Phys. Rev. Lett.* **58**, 2131 (1987); *J. Chem. Phys.* **86**, 1167 (1987).
- [42] J. K. G. Watson in Vibrational Spectra and Structure, J. R. Durig, Ed., Vol. 6, Chap. 1 (Elsevier, New York, 1977).
- [43] "A reduced form of the spin-rotation Hamiltonian for asymmetric-top molecules with applications to HO_2 and NH_2 ." J. M. Brown and T. J. Sears, *J. Mol. Spectr.* **75**, 111 (1979).
- [44] "The vibration-rotation fundamental of NO." Johns, Reid, Lepard, *J. Mol. Spectr.* **65**, 155 (1977); "Microwave spectral tables I. Diatomic molecules." F. J. Lovas and E. J. Tiemann, *J. Phys. Chem. Ref. Data* **3**, 609 (1974).
- [45] "Emission spectra in a supersonic expansion: The quartet system of NO and the Schuler band of ND_4 ." K. P. Huber and T. J. Sears, *Chem. Phys. Lett.* **113**, 129 (1985).
- [46] "Magic losses from metastable N_3^+ clusters as a statistical evaporation process." P. C. Engelking, *Chem. Phys. Lett.* **139**, 6 (1987).
- [47] "Photodetachment cross sections of negative ions: The range of validity of the Wigner Threshold Law." J. W. Farley, *Phys. Rev.* **A40**, 6286 (1989).

**END
FILMED**

DATE:

11 - 90

DTIC